

A Bayesian-based inspection-monitoring data fusion approach for historical buildings and its post-earthquake application to a monumental masonry palace

Laura Ierimonti^{1*}, Nicola Cavalagli¹, Ilaria Venanzi¹, Enrique García-Macías^{1,2} and Filippo Ubertini¹

^{1*}Department of Civil and Environmental Engineering,
University of Perugia, Via G. Duranti, Perugia, 06125, Italy.

²Department of Structural Mechanics and Hydraulic Engineering,
University of Granada, Av. Fuentenueva sn, Granada, 18002,
Spain.

*Corresponding author(s). E-mail(s): laura.ierimonti@unipg.it;
Contributing authors: nicola.cavalagli@unipg.it;
ilaria.venanzi@unipg.it; enrique.garciamacias@unipg.it;
filippo.ubertini@unipg.it;

Abstract

Many countries exposed to high levels of seismic risk, including Italy, are facing a huge challenge in promptly quantifying post-earthquake damages to their built historical heritage. In this context, structural health monitoring (SHM) plays a fundamental role allowing to continuously track changes in selected damage-sensitive features. However, monitoring data interpretation is often not univocal and may be affected by large uncertainty, provoking false positives and false negatives. Hence, this research proposes a novel approach for post-earthquake structural condition assessment by exploiting the aggregation of different sources of information, notably steering from both monitoring and visual inspection campaigns, in order to take risk-informed decisions. More in depth, an automatic tool is proposed to detect and locate structural damages in monumental structures with the aid of a data fusion approach including vibration-based system identification, static and dynamic measurements, finite element (FE) and surrogate modeling, Bayesian-based

model updating and visual inspections.

In a preliminary phase, potential damage-sensitive regions in the structure are identified through FE-based numerical analysis and engineering judgment. Then, the solution of the inverse problem aimed at deriving the Bayesian posterior statistics of the uncertain parameters is entrusted to a computational-effective surrogate model (SM). Finally, the Bayesian-based updated parameters are adjusted considering the different allowable sources of information to achieve a final assessment. The effectiveness of the proposed approach is demonstrated by using the recorded data acquired in the Consoli Palace, an historical building located in Umbria, central Italy, which has been continuously monitored since 2017 using dynamic, static and environmental sensors and which has been hit by low-intensity earthquakes in 2021.

Keywords: Data fusion, Bayesian model updating, surrogate modeling, post-earthquake damage classification, continuous monitoring, historic masonry construction

1 Introduction

Structural damages suffered by monumental structures have confirmed that those types of buildings are especially prone to aging problems, material's degradation, earthquakes, foundation settlements and more. Hence, non-destructive SHM-based testing techniques are spreading out [1], focusing the attention on evaluating the structural condition continuously over time in order to properly plan restoration interventions. Usually, damage identification can be defined as a five-level hierarchical problem [2], which consists of: (i) detection; (ii) localization; (iii) classification ; (iv) assessment; (v) prediction. Conventional SHM-systems typically allow to capture modifications of the global behavior of the structure (novelty detection), which essentially represents step (i) above. Indeed, structural modal parameters can be related to material's damage and deterioration [3–7], with a specific attention to the evaluation and the removal of the effects of changing temperature and humidity [8]. Recent contributions deal with long-term SHM data and damage detection [9–14]. A brief review on SHM for data-driven damage identification problems is given in [15]. An efficient tool for the design of the monitoring system as well as the rapid post-earthquake damage assessment of precast reinforced concrete industrial buildings is proposed in [16]. Several works achieve the SHM-based damage assessment by making use of Bayesian model updating techniques, in order to deal with different sources of uncertainty [17–22]. For this purpose, the use of surrogate models can be considered as a valid tool for handling uncertainties and reducing the computational effort [23, 24]. Furthermore, probabilistic frameworks based on machine learning techniques are explored in literature encompassing the SHM field [25–29].

As confirmed by the literature review, the complex nature of the real-world

applications leads to high levels of uncertainties during the data pre-processing and post-processing stages. This is especially true in the case of complex masonry buildings, where both local and global damage mechanisms may activate and where an accurate numerical modeling is always a challenge, especially when it comes to the non-linear range of behavior. In this context, making assessments based on heterogeneous sources of information becomes imperative. In particular, multisensory SHM systems, including both static and dynamic, local and global features, as well as visual inspections and engineering judgements need to be part of an overall structural assessment strategy that can reduce uncertainties and allow making robust decisions. As reported in [30], a multi-sensor-based approach can be designated as data fusion, a class of methods capable of combining information from several sources in order to form a unified picture.

The concept of data fusion has been widely applied in various research fields such as environmental monitoring, robotics, medical applications, quality control of manufacturing process and condition monitoring of complex machinery [31]. Different works in the literature interface with data fusion approaches in order to estimate the potential risk of damage as well as detect and quantify a damage after a critical event. An overview of the state-of-the-art algorithms implementing data fusion is presented in [15, 30–32].

Different levels of data fusion can be recognized [33]: (i) data-level; (ii) feature-level; (iii) decision-level. Each level is schematically represented in Figure 1. The data-level fusion consists of directly combining the raw data from multiple sources in the pre-processing phase. At this level it is necessary that all the raw data have the same physical meaning. The feature-level fusion can gather together heterogeneous input data which are conveniently concatenated prior (feature extraction) to further analysis. Finally, in decision-level fusion all the data are separately investigated and the final decision is achieved by means of selected combination rules (feature extraction and intermediate results). Different works in literature embrace data fusion and a brief overview is presented below. In [34] a transformed Subspace State-Space System Identification (SSID) and the Unscented Kalman Filter methods are compared with their ability to localize damage including fusion of heterogeneous sources. In [35] a technique to fuse sensor data into a single damage detection feature is proposed, providing a simple and robust method for inspecting large numbers of sensors without the need for complex model-driven approaches. A two-stage structural damage detection approach using fuzzy neural networks (FNNs) and data fusion techniques is proposed in [36]. In [37] an automated technique is developed for residential buildings to yield a robust decision regarding the attributes and condition of a target structure by fusing the results obtained from several images. The results presented in [38] demonstrate the possibility to have a better design of the SHM system for the damage localization where the benefits of different damage indices and evaluation methodologies are explored by means of fusion of the identified results. In [39] a framework is presented to support fusion of multiple nondestructive evaluation techniques

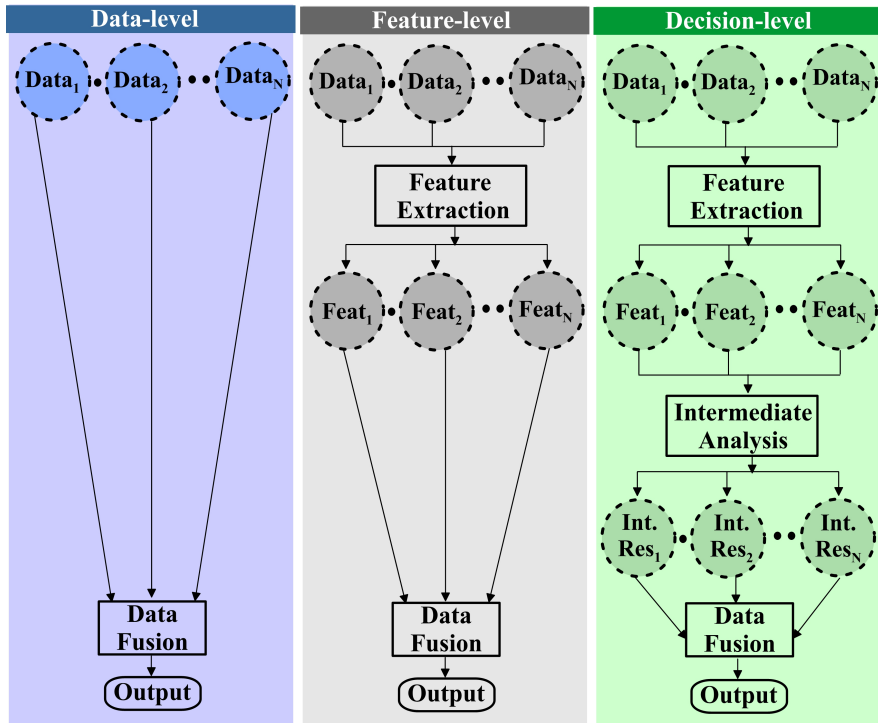


Fig. 1 The different levels of data fusion [33]: data-level, feature-level, decision-level.

in order to improve both detection and quantification accuracy while also improving the visualization of NDE results. In [40] a multi-source Bayesian framework is applied by fusing information obtained from crack growth rate monitoring using acoustic emission, empirical crack growth model and periodic inspections. In [41] a methodology based on the Bayesian data fusion techniques applied to non-destructive and destructive tests for the structural assessment of historical constructions is developed. The advantage of having global (such as frequencies and mode shapes) and local (such as static strain, crack amplitude and tilt rotation) information for damage detection is explored in [42]. An automated SHM-based approach by simultaneously interpreting data from a distributed sensor network in a civil infrastructure is proposed in [43]. From the literature review it points out that an efficient methodology capable of post-processing data by combining heterogeneous sources, including visual inspections, to make robust decisions still remains a challenge and a further research effort is needed. In particular, the idea is to overstep the existing gap between real-world inspection surveys, expert judgment and numerical predictions made exploiting SHM data, going towards standard protocols. On the one hand, the sole numerical predictions are often ill-posed, since the solution of detected anomalies might be not unique or does not depend continuously on the data. On the other hand, the sole visual inspections might disregard some

structural anomalies, not clearly visible but captured by continuous SHM. Finally, expert judgment and Bayesian model updating contribute to overcome the main issue related to the unsupervised SHM, e.g., damage localization.

In this context, a decision-level-based methodology is presented, which includes fusion of heterogeneous sensors, expert judgment and visual inspections, with the main objective of formally aggregating all these independent sources of information to achieve a more accurate assessment of the health of a masonry structure after an earthquake by increasing reliability and improving defect detection.

The case study is the Consoli Palace located in Gubbio, near Perugia, in Italy, a complex historical masonry building. The structure has been monitored by the Authors since 2017 and the SHM sensors' network has been enhanced in 2020. The results show the advantage of having long-term monitoring data combined with visual inspections to improve confidence in damage identification.

The main novelties introduced in the present paper can be summarized as follows:

- the fusion system architecture combines different sources of information in a mathematically sound manner,
- Bayesian inference is used in fusing monitoring and visual inspection information to mitigate uncertainties,
- the FE model and its surrogate representation allow to identify critical factors which can affect the outcome of the SHM-based post-processing data analysis,
- the visual inspections and static measurements allow to improve accuracy and reliability of results, clarifying the role of any modal features (MF) variation in the structure and avoiding misleading results.

The rest of the paper is organized as follows. Section 2 presents the proposed methodology for continuous SHM and Bayesian model updating. Section 3 describes the monumental building selected as case study, the continuous monitoring system and the numerical models. Section 4 illustrates the results and, finally, Conclusions are drawn in Section 5.

2 Multi-source Bayesian-based data fusion

The sequential steps of the proposed methodology are summarized in Fig. 2 and itemized as follows:

1. FE modeling and updating based on results of Ambient Vibration Tests (AVT) and in situ material characterization tests.
2. Evaluation of damage-sensitive portions of the building on the basis of nonlinear static analysis (NLSA) and Engineering judgment.
3. Calibration of a SM as a function of the uncertain parameters to be updated associated to each damage-sensitive structural macro-element.

6 *A Bayesian-based inspection-monitoring data fusion approach*

4. Continuous SHM. Data acquisition from the monitoring system which typically comprises acceleration/velocity data, temperature/humidity data and static measurements, such as crack amplitudes and tilt rotations.
5. Features extraction, i.e., continuous post-processing over time of the available data: (i) vibration-based data in order to estimate the modal features associated with the i^{th} natural vibration mode from operational modal analysis; (ii) static measurements, such as crack amplitudes; (iii) environmental measurements, i.e., temperature and/or humidity;
6. Novelty detection through the use of statistical pattern recognition methods. If a Novelty is detected, e.g. after an earthquake, perform the Bayesian model updating and proceed with visual inspection in order to identify possible structural damages. If a Novelty is not detected, go back to the beginning of point 3.
7. Intermediate analysis. Perform the Bayesian model updating and assign the Bayesian index (BI). Proceed with visual inspections and evaluate the damage index (DI). Analyze data derived from static measurements and assign the crack index (CI). The indexes BI, DI, CI are associated with each selected damage-sensitive portions of the structure.
8. Data Fusion, i.e., adjust the posterior statistics by means of data fusion, e.g., combine the information derived from visual inspections (DI), measured static data (CI) and Bayesian-based results (BI).

2.1 FE modeling

The FE modeling plays a key role in the proposed procedure in order to predict and understand how the structure might behave under various physical conditions. A numerical model \mathcal{M} of the structure is built and calibrated on the basis of expert judgment, documents available from archival sources and in-situ inspections. The calibration procedure of \mathcal{M} consists of several steps aimed at minimizing the difference between numerical and experimental responses. In this work, modal characteristics are considered for this purpose and the model updating problem is formulated as follows:

1. Identify the dynamic behavior of the structure, i.e., the frequency f_i^{exp} , the mode shape Φ_i^{exp} and damping ratio ζ_i^{exp} associated with each i^{th} fundamental mode by means of AVTs with a dense sensor's network;
2. Construct the FE model of the structure as a function of the vector $\mathbf{Y} = \{\mathbf{Y}_1, \dots, \mathbf{Y}_u, \dots, \mathbf{Y}_U\}$ collecting parameters to be calibrated (for $i=1,2,\dots,M$, where M is the number of identified modes). In the context of this paper, \mathbf{Y}_u is the vector collecting the Young's modulus E , shear modulus G , Poisson's ratio ν and mass density w of the materials of pre-defined structural macro-elements;
3. Perform the modal analysis and evaluate each FE-based i^{th} natural frequency f_i^{FEM} and mode shape Φ_i^{FEM} (for $i=1,2,\dots,M$);

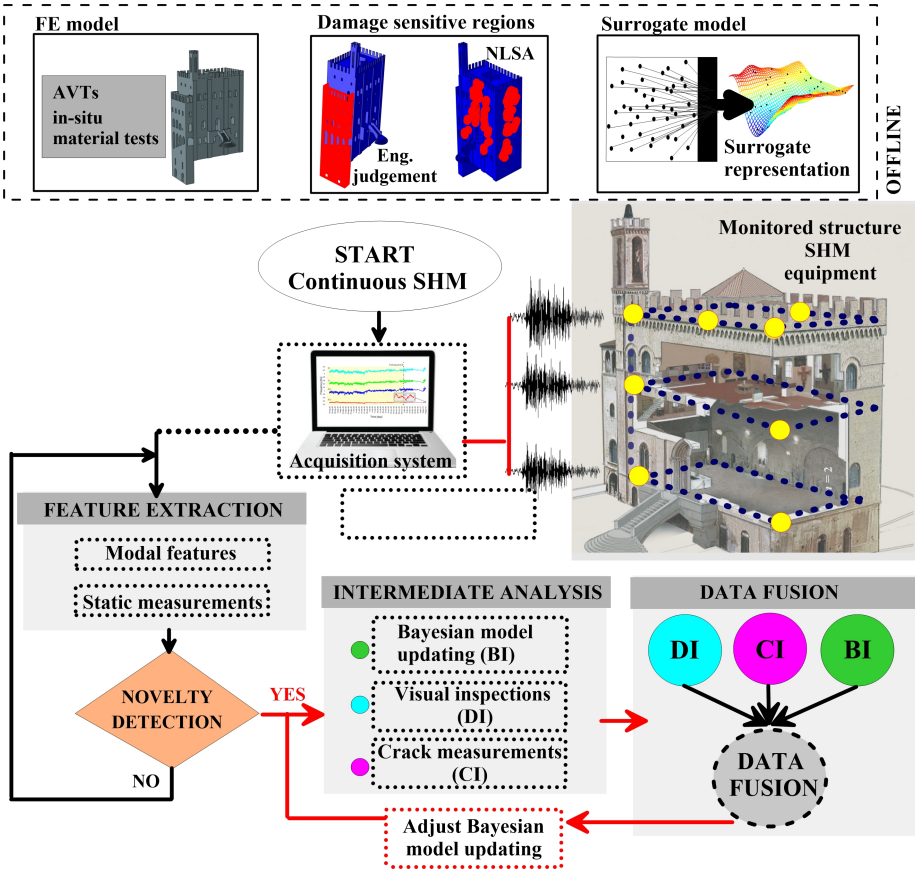


Fig. 2 The proposed data fusion Bayesian-based methodology.

4. Solve the optimization problem: calculate the optimum values of the uncertain parameters \mathbf{Y}^{opt} via solving the following optimization problem:

$$\mathbf{Y}^{\text{opt}} = \arg \min_{\mathbf{Y} \in \mathfrak{D}} \sum_{i=1}^M p_1 \eta_{f,i}(\mathbf{X}) + p_2 \eta_{\Phi,i}(\mathbf{Y}) \quad (1)$$

where p_1 and p_2 represent the weights of the objective function; $\eta_{f,i}(\mathbf{Y}) = |f_i^{\text{exp}} - f_i^{\text{FEM}}| / f_i^{\text{exp}}$; $\eta_{\Phi,i}(\mathbf{Y}) = 1 - \text{MAC}_i(\mathbf{Y})$; MAC_i indicates the Modal Assurance Criterion (MAC) between the i^{th} experimental and numerical mode shapes;

Besides the calibration of the elastic constants, the characterization of the parameters of the damage model has to be carried out through the support of non-invasive diagnostic investigations [8].

2.2 Identification of damage-sensitive regions

In order to define the damage-sensitive macro-elements, it is appropriate to locate possible critical areas with respect to different damage mechanisms, such as materials aging, foundation settling, local mechanisms and more on the basis of Engineering judgment. Then, to accommodate for global damage mechanisms, linear and/or nonlinear analyses can be used to numerically identify structural regions that are critical with respect to mechanical damage mechanisms associated to vertical and horizontal loads, such as dead loads and earthquakes. The main goal is to select N damage-prone regions $\mathcal{R} = \{\mathcal{R}_1, \dots, \mathcal{R}_j, \dots, \mathcal{R}_N\}$. Hence, the j th region can be considered as an homogeneous macro element in terms of material's mechanical characteristics and the vector $\mathbf{X}(\mathcal{R}) = \{k_1(\mathcal{R}_1), \dots, k_j(\mathcal{R}_j), \dots, k_N(\mathcal{R}_N)\}$ collects the damage parameters which represent the multipliers of the Young moduli (k_j) of all the micro-elements comprised in each region, with $0 \leq k_j \leq 1$. For the sake of simplicity, the dependence on \mathcal{R} in the term $\mathbf{X}(\mathcal{R})$ is dropped hereafter.

2.3 Surrogate modeling

With the main objective of reducing the computational effort of the Bayesian-based process, a SM is trained to reproduce the dynamic behavior of the structure as a function of $\mathbf{X}(\mathcal{R})$. Among all the numerical surrogate models available in literature, the Kriging model is considered given its largely documented effectiveness and computational efficiency [16, 23].

A Kriging model is a generalized linear regression model that uses a limited set of sampled data points to estimate the value of the uncertain variables over a continuous spatial field accounting for the mismatch between the regression model and the observations. More details can be found in [16, 23, 44]. In the present work, the Kriging-based model is used to provide the explicit function to represent the relationships between frequencies, mode shapes and uncertain parameters \mathbf{X} . Then, in order to measure how well the SM replicates the FE model, the coefficient of determination R^2 can be evaluated [45]:

$$R^2 = 1 - \frac{\sum_T (y_T^* - y_T)^2}{\sum_T (y_T - \bar{y})^2} \quad (2)$$

where T is the dimension of the training population; y_T^* is the prediction for the T^{th} instance of the surrogate model, y_T collects the T^{th} FE model's value and \bar{y} is the mean of the SM predictions. The R^2 represents the percentage of variance that is captured by the SM. Indeed, if R^2 is close to 1 it means that the SM well approximates the behavior the FE model very well, while if R^2 approaches 0 the SM fails.

Furthermore, an index named J_{MAC} can be introduced to estimate the

consistency of modal shapes:

$$J_{\text{MAC}} = 1 - 1/N_s \sum_i (1 - \text{MAC}_i) \quad (3)$$

with N_s number of samples, i.e., the number of mode shapes considered in the analysis. The surrogate model well represents the FE-based mode shapes the more J_{MAC} approaches 1.

2.4 Feature extraction

In order to investigate continuously over time the modal features, an automated tool based on the covariance-based stochastic subspace identification (SSI) technique, implemented in MOSS integrated software [46, 47], is used to convert vibration data into modal properties.

In order to avoid ambiguous results, environmental effects are removed from original signals by means of statistical models after analyzing the time series of ambient and material temperature measurements during the training period, typically 1 year. ~~In this study, the Multiple Linear Regression (MLR) is used to predict the values of the post processed data. More in detail, the Least Angle Regression (LAR) algorithm [48] and the Bayesian Information Criterion (BIC) are implemented and used to identify the optimal set of predictors among all the generated models.~~ A classical approach for novelty detection uses control charts and statistical measures. For the present paper, the presence of damage, e.g. anomalies in ~~the residual $E(t)$ evaluated at time t ,~~ is calculated by means of the Hotellings T^2 control chart [49], where the novelty is related to the estimation of the square Mahalanobis distance T^2 of the residuals. The Mahalanobis distance is a statistical measure able to consider both the distance of the i th observation from the centroid of the data, and the shape of the data. T^2 can be defined as follows:

$$T^2(t) = (E(t) - \bar{E})^T \Sigma^{-1} (E(t) - \bar{E}) \quad (4)$$

where \bar{E} represents a vector collecting the mean values of the residuals empirically estimated in the training period and Σ the corresponding covariance matrix.

2.5 Intermediate analysis

2.5.1 Bayesian-based model updating

The Bayesian model updating at time t is used for evaluating the posterior statistics $p(\mathbf{X}(\mathcal{R}) \mid \mathbf{d}, t, \mathcal{M})$ of the uncertain parameters $\mathbf{X}(\mathcal{R})$ defined in Sect. 2.1, conditional on the experimentally measured data $\mathbf{d}(t)$, i.e., observations, and a selected mathematical model \mathcal{M} by means of the likelihood of measured

data and the prior knowledge acquired at $t - 1$. The general formulation can be obtained by the Bayes theorem as follows:

$$p(\mathbf{X}(\mathcal{R}) \mid \mathbf{d}, t, \mathcal{M}) = c \cdot p(\mathbf{d} \mid \mathbf{X}(\mathcal{R}), t, \mathcal{M}) \cdot p(\mathbf{X}(\mathcal{R}) \mid t, \mathcal{M}) \quad (5)$$

where:

- $p(\mathbf{d} \mid \mathbf{X}, t, \mathcal{M})$ is the likelihood function of the data \mathbf{d} and indicates how likely the measured data are reproduced by the numerical model;
- $c = 1 / \int p(\mathbf{d} \mid \mathbf{X}(\mathcal{R}), t, \mathcal{M}) p(\mathbf{X}(\mathcal{R}) \mid \mathcal{M}) d\mathbf{X}(\mathcal{R})$ is the evidence of the model class \mathcal{M} ensuring that the posterior PDF integrates to 1;
- $p(\mathbf{X}(\mathcal{R}) \mid t, \mathcal{M})$ is the prior distribution of $\mathbf{X}(\mathcal{R})$, i.e., the a-priori knowledge on the uncertain parameters, evaluated as the posterior distribution at $t - 1$ $p(\mathbf{X}(\mathcal{R}) \mid \mathbf{d}, t - 1, \mathcal{M})$.

In the present work, the uncertain parameters k_j collected in vector $\mathbf{X}(\mathcal{R})$ are assumed as statistically independent [9, 50], meaning that they are separately updated over time and Eq. (5) can be rewritten as follows:

$$p(k_j \mid \mathbf{d}, t) = c \cdot p(\mathbf{d} \mid k_j, t) \cdot p(k_j \mid \mu(t - 1)) \quad (6)$$

As can be deduced from Eq. (6), the standard deviation of the prior distribution is assumed as known, while the mean value μ is updated step by step. This assumption guarantees to correctly and promptly identify a possible damage occurrence, even in the case of a large number of "undamaged" monitoring data. Indeed, the large amount of data might make the prior barely sensitive to the occurrence of damage due to a small standard deviation (or variance) at time $t - 1$, meaning that the distribution of the uncertain parameter is narrowly concentrated around the mean (undamaged value). Instead, the updating of the sole mean value μ can give information on which value of damage-sensitive parameter is more plausible or believable, given the evidence of new data $\mathbf{d}(t)$ and, consequently, which region might be subjected to damage.

Particular care has to be given to the definition of the likelihood function to ensure that the model updating produces relevant variations in the prior knowledge. In the present paper, the likelihood is modeled as a Gaussian distribution with zero mean, as in [9, 16, 50]. More details in the numerical formulation are given in [16].

For completeness, a probabilistic damage identification is associated to the Bayesian model updating. In particular, according to [9, 51], the probability P_j^{dam} that the updated j th parameter k_j^{up} in a possibly damaged state is reduced from the undamaged state k_j^{ref} can be written as:

$$P_j^{\text{dam}} = P(k_j^{\text{up}} \leq (1 - \bar{k}_j)k_j^{\text{ref}} \mid \mathbf{d}^{\text{ref}}, \mathbf{d}^{\text{dam}}) = F \left(\frac{(1 - \bar{k}_j)k_j^{\text{ref}} - k_j^{\text{up}}}{\sqrt{(1 - \bar{k}_j)^2 \sigma_{k_j^{\text{ref}}}^2 + \sigma_{k_j^{\text{up}}}^2}} \right) \quad (7)$$

where $F(\cdot)$ is the standard Gaussian cumulative distribution function, $\bar{k}_j \in [0, 1]$, which represents the reduction of k_j^{ref} , is a damage threshold selected for the j th damage-prone region and $k_j^{\text{ref}} = 1$ is the reference undamaged state. Changes in P_j^{dam} are studied as a sign of possible damage and the probability-based damage threshold is designated as P_j^{al} , as specified in Table 1.

Additionally, a damage factor DF can be introduced as:

Case No.	k_j^{up}	P_j^{dam}	Meaning
1	$= (1 - \bar{k}_j)k_j^{\text{ref}}$	$= 0.5$	damage threshold reached $P_j^{\text{dam}} = P_j^{\text{al}}$
2	$> (1 - \bar{k}_j)k_j^{\text{ref}}$	< 0.5	damage threshold not reached
3	$< (1 - \bar{k}_j)k_j^{\text{ref}}$	> 0.5	damage threshold exceeded

Table 1 Probability-based damage identification, possible values of k_j^{up} and P_j^{dam} .

$$DF = \frac{k_j^{\text{ref}} - k_j^{\text{up}}}{\bar{k}_j} \quad (8)$$

From Eq. (8) it is possible to obtain DF=0 (undamaged) if $k_j^{\text{up}} = k_j^{\text{ref}}$ and DF=1 if $k_j^{\text{ref}} - k_j^{\text{up}} = \bar{k}_j$ (damaged). Otherwise, DF increases with values higher than 1 as \bar{k}_j tends to zero, meaning that the damage might be completely developed. However, given the complexity of the problem, there is always the risk of incurring in a false alarm. In order to tackle this problem, a data fusion strategy is proposed in this paper where heterogeneous information is used to achieve more reliable predictions. Hence, it is appropriate to assign a coefficient, named Bayesian Index BI, to the Bayesian-based results, i.e., assign BI=1 if the updated values are reduced more or equal 10 % with respect to the undamaged state, otherwise assign BI=0;

2.5.2 Visual inspections

The level of knowledge of a masonry structure in terms of structural and geometrical properties depends on many factors including the structural knowledge at the time of construction, the experience of the inspector, the seismic hazard of the site, just to mention the most influential parameters [52]. Furthermore, the use or occupancy of the structure may vary over time inducing unexpected loads. Hence, structural damage, failure or total structural collapse may occur suddenly during moderate or strong earthquakes. Thus, it is essential to evaluate the capacity of existing historical structures through on-site inspections designed to estimate safety and usability of the building in order to eventually plan further relief and retrofit measures [53] before an earthquake strikes. This stage should be carried out through a rapid screening, filling out easily understandable and standard forms.

As a support for the purpose, a detailed catalogue of the main damages on masonry buildings is reported in MEDEA (Manual for Earthquake Damage

Evaluation and safety Assessment) tool [54]. In the aforementioned catalogue two principal mechanisms are identified: 1) global mechanisms (reported in Table 2) affecting the whole structure and related to the evolution of crack patterns in a number of elements sufficient to compromise the static and dynamic equilibrium of the structural system; 2) local mechanisms (reported in Table 3) affecting marginal parts of the structure and whose evolution generally affects the individual element and does not compromise the global structural behavior.

Furthermore, field inspections results can be numerically quantified [55, 56] and, for the purpose, a damage index DI is proposed in order to determine the damage of the j th region:

$$DI_j = \sum_{i=1}^m G_{ji} \cdot K1_{ji} \cdot K2_{ji} \quad (9)$$

where m is the the total number of damages associated with the j th region, G stands for the weight (importance) of the damage, $K1$ describes its extension and $K2$ its intensity. The numerical values associated to the aforementioned coefficients are summarized as follows:

- $G=0$ absence of damage; $G=1$ local mechanism; $G=5$ global mechanism, as reported in Tables 2 and 3.
- $K1=0.2$ restricted extension; $K1=0.5$ relevant extension; $K1=1$ the damage is affecting the whole element/region.
- $K2=0.2$ minor intensity; $K2=0.5$ medium intensity; $K2=1$ the damage is completely developed.

For data fusion purposes, a region is considered "damaged" if $DI > 0$.

In this context, a general guide for the visual inspection is here proposed, developed according to the information provided in MEDEA [54] and in the Applied Technology Councils Procedures for Post-earthquake Safety Evaluation of Buildings documents [57–59], which represent a complete guideline for post-earthquake safety inspections of buildings by assigning a classification tag that designates the building structural condition.

More in depth, a visual inspection form should be filled for each predefined macroelement of the building enabling a rapid post-earthquake structural safety assessment by conferring a green, yellow or red classification tag, corresponding to different safety levels, which can be summarized as follows [16]:

- INSPECTED, i.e., apparently safe, corresponding to a green classification tag (GT);
- RESTRICTED USE, corresponding to a yellow classification tag (YT);
- UNSAFE, corresponding to a red classification tag (RT).





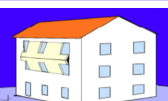
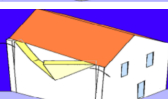



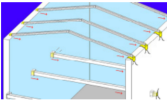
Mech. No.	Mech. type	G	Graphical representation
1	shear mechanisms	5	
2	upper levels storey shear mechanisms	5	
3	whole wall overturning	5	
4	partial wall overturning	5	
5	wall vertical instability	5	
6	wall bending rupture	5	
7	horizontal sliding failure	5	
8	foundation failure	5	
9	irregularity between adjacent structures	5	
10	floor and roof beam unthreading	5	

Table 2 Masonry-dependent global mechanisms [54].

2.5.3 Static measurements

The influence of the static measurements is evaluated by means of an index, designated as crack index CI, evaluated for each region potentially involved. More in detail, assign CI=1 if the crack measurement exhibits a permanent closure or opening, otherwise assign CI=0.

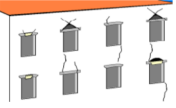


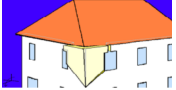
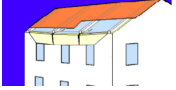

Mech. No.	Mech. type	G	Graphical representation
11	lintel or masonry arch failure	1	
12	material irregularity, local weakness	1	
13	roof gable wall overturning	1	
14	corner overturning in the upper part	1	
15	overturning of the wall supporting the roof	1	
16	vault and arch overturning	1	

Table 3 Masonry-dependent local mechanisms [54].

2.6 Data fusion

The main idea behind this work is to propose a method combining information from both visual inspections and monitoring-based model updating data, since the sole model updating problems might be subjected to ill-posedness and ill-conditioning issues, especially because of a large number of potential damage patterns and because of measurement noise. Hence, all the information sources are combined as follows: calculate the data fusion results on the basis of indexes BI, DI and CI by means of the well-known 2-out-of-3 (2oo3) method [60], named 2oo3 voter, on the basis of majority, i.e., assign 1 if the specific region has the majority of BI, DI and CI higher than 0, assign 0 otherwise. In the absence of crack information for a specific region, the value of DI is counted twice.

Then, the posterior value of k_j^{up} is adjusted by means of a correction coefficient Ψ_j^{VI} on the basis of the 2oo3 voter as follows:

$$k_j^{\text{up,VI}} = \Psi_j^{\text{VI}} \cdot k_j^{\text{up}} \quad (10)$$

where $k_j^{\text{up,VI}}$ is the updated value of the damage-sensitive parameter after data fusion (Bayesian model updating and visual inspection). The coefficient Ψ_j^{VI} can assume the following values:

- If the 2003 voter is 1 (damaged state), $\Psi_j^{VI} = 1$
- If the 2003 voter is 0 (undamaged state), $\Psi_j^{VI} = k_j^{\text{ref}}/k_j^{\text{up}}$.

This methodology allows a prediction of damage to be made, based on Bayesian numerical simulations, progressively updated with new information collected during visual surveys.

3 The case study

3.1 Description of the Consoli Palace and the monitoring system

The Consoli Palace is one of the most audacious architectural complexes constructed in the 14th century and is located in Gubbio, Umbria, central Italy. Since 1909 the Consoli Palace has housed the Civic Museum whose collections illustrate the history and culture of Gubbio and its community. The palace, with its 60 m of height, overlooks the main square of the town, suspended on an arched structure. It is accessed through a staircase and it is composed by a central body, a panoramic loggia and a bell tower. Figs. 3a)-c) illustrate some architectural details of the structure. The East and West side façades are characterized by round arched windows and merlons in the rooftop. The load-bearing walls have a thickness of about 1.2 m and each floor of the building is characterized by vaulted ceilings, differently oriented and distributed. The Palace is built in calcareous stone masonry with a regular and homogeneous texture.

According to the Italian technical standard NTC2018 [61], Gubbio is assigned to the seismic area 2, which is characterized by $0.15 < \text{PGA} \leq 0.25$, PGA being with a probability of exceeding of 10% in 50 years. The city is located near the Gubbio normal fault, a 22-km-long pre-orogenic fault reactivated in a post-orogenic stage [62]. The high seismicity of the area is constantly monitored by a dense network of seismic stations (Alto Tiberina Near Fault Observatory - TABOO) [63].

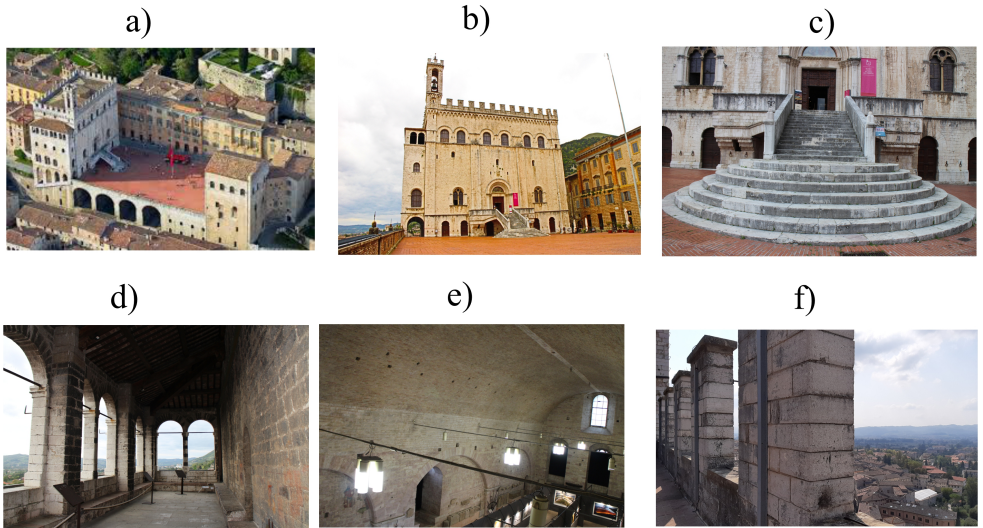


Fig. 3 The case study: a) aerial view; b) main façade; c) staircase; d) loggia; e) horizontal masonry vaults; f) rooftop.

A continuous monitoring system was installed in 2017 with an improvement in terms of number of sensors in July 2020. The system has been designed and managed by the Department of Civil and Environmental Engineering of University of Perugia in the context of European and National projects. The system, schematically illustrated in Fig. 4, is composed by: a mixed data acquisition system to which some sensors are wired (model NI CompactDAQ-9132 equipped with NI 9234 acquisition modules for accelerometers with 24-bit resolution, 102-dB dynamic range, and anti-aliasing filters, and NI 9219 acquisition modules with 24-bit resolution, ± 60 V range, 100 S/s for LVDTs and thermocouples) and a wireless network (LoRaWAN system technology); twelve unidirectional accelerometers A1-A12 (model PCB393B12 with a measurement range \pm of 0.5 g, a frequency range of 0.15-1000 Hz, a broadband resolution 8 μ g and a resonant frequency ≥ 10 kHz); four linear variable transducers D1-D4 (model S-series with a measurement range of 0-0.5 mm and a resolution of 0.31 m) and six thermocouples T1-T6 (model K-type).

Acceleration data are stored in 30 min-long files with a sampling frequency of 40 Hz, while crack amplitudes and temperature values are sampled every 30 minutes. Data are continuously saved in a cloud storage and can be accessed through a web-based platform.

With the main objective of evaluating the dynamic characteristics of the building for finite element model updating purposes, an AVT was carried out on the Consoli Palace on May 7th, 2021 by adding channels A13-19 (Fig. 4). The channels A13-A16 allow to better define the rooftop dynamic behavior and channels A17-A19 permit to characterize the role of the bell tower in the dynamic identification. The main characteristics of the sensors' network are

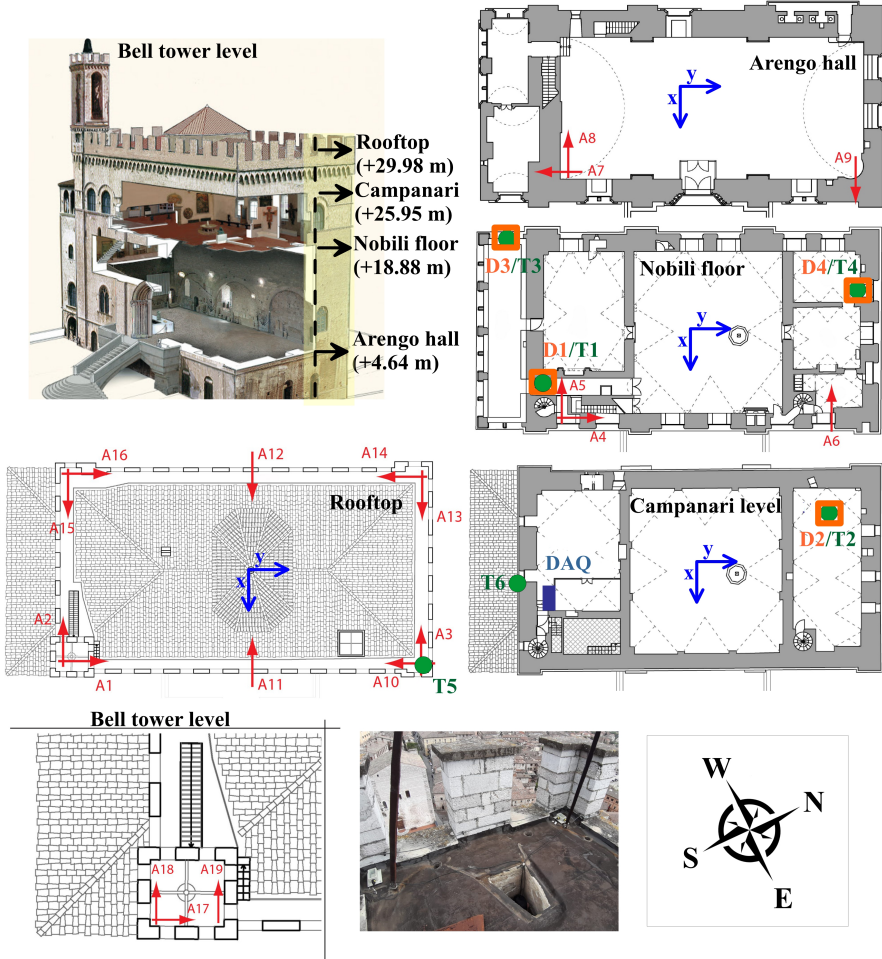


Fig. 4 Schematic representation of the SHM system.

summarized in Table 4. Finally, Fig. 5 illustrates the experimental set-up of channels A1-A19.

The identified modes and the comparison between the experimentally identified frequencies during the AVT and the continuous SHM are summarized in Table 5. More details on the dynamic identification were given in [8, 64] and then upgraded in [65].

It is worth noticing that the bell tower plays a fundamental role in the dynamic identification of the structure. Indeed, as reported in [65], both local and global modes are found in the range from 0 to 10 Hz, i.e., Ly_1 - Lx_1 and Fy_1 , due to the high complexity of the structure.

Channel	Level	Measure	Direction	SHM	AVT
A1	rooftop	acceleration	y	•	•
A2	rooftop	acceleration	x	•	•
A3	rooftop	acceleration	y	•	•
A4	Nobili	acceleration	y	•	•
A5	Nobili	acceleration	x	•	•
A6	Nobili	acceleration	y	•	•
A7	Arengo	acceleration	$-y$	•	•
A8	Arengo	acceleration	x	•	•
A9	Arengo	acceleration	$-x$	•	•
A10	rooftop	acceleration	$-y$	•	•
A11	rooftop	acceleration	x	•	•
A12	rooftop	acceleration	$-x$	•	•
A13	rooftop	acceleration	$-x$	•	•
A14	rooftop	acceleration	$-y$	•	•
A15	rooftop	acceleration	$-x$	•	•
A16	rooftop	acceleration	y	•	•
A17	bell tower	acceleration	y	•	•
A18	bell tower	acceleration	x	•	•
A19	bell tower	acceleration	x	•	•
D1-D3-D4	Nobili	crack's length	—	•	•
D2	Campanari	crack's length	—	•	•
T1-T3-T4	Nobili	temperature	—	•	•
T2-T6	Campanari	temperature	—	•	•
T5	rooftop	temperature	—	•	•

Table 4 SHM and AVT sensors' network within the building.

Mode no.	Label	Mode type	f_{AVT} [Hz]	\bar{f}_{SHM} (\pm var. range) [Hz]
1	Fx1	flexural mode along x	2.32	2.32 (-5.80%+5.10%)
2	Ly1	bell tower's local mode along y	2.99	3.02 (-8.65%+14.29%)
3	Lx1	bell tower's local mode along x	3.54	3.53 (-8.54%+14.10%)
4	Fy1	flexural mode along y	3.75	3.75 (-6.36%+5.77%)
5	T1	torsional	4.2	4.2 (-8.28%+7.34%)
6	Fx2	flexural mode along x	5.65	5.53 (-7.78%+8.02%)
7	LT1	bell tower's torsional mode	5.91	6.46 (-7.75%+8.27%)

Table 5 Comparison between the experimentally identified frequencies during the AVT and the continuous SHM.

3.2 FE/surrogate model calibration

In order to account for the results obtained by the AVTs on May 2021, the FE model of the structure, as presented in [8, 16], has been adjusted by solving the optimization problem introduced in Eq. (1) with $u = 9$ and $\mathbf{Y} = \{k_1, \dots, k_9\}$, meaning that the model has been sub-divided in 9 regions, as is depicted in Fig. 6: R1 comprises the Arengo floor and the underlying areas; R2 represents the Nobili arched ceiling; R3 the rooftop and its annexes; R4 the loggia; R5 the bell tower; R6 and R7 the potential cracking patterns that can be activated by an earthquake evaluated as reported in [16] through non-linear static analysis (NLSA); R8 the vertical walls along the x direction; R9 the vertical walls along the y direction. An isotropic material is assigned to each macro-element of the FE model and the non-linear behavior of the material is reproduced by using the well known concrete damage plasticity (CDP) model, introduced



Fig. 5 Pictures of A1-A19 channels.

in [66]. The nominal values of the parameters associated to the FE model-based macro-elements and k_j values after calibration are reported in Table 7. From the results it can be noted that $k_4 = 0.8$ representing the poor connection between the loggia and the central body of the palace. The parameter $k_5 = 1.4$ reflects the actual structural condition of the bell tower characterized by recent metallic internal reinforcement installed during the repairing of damages caused by past earthquakes. Parameters k_6 and k_7 equal to 0.6 agree well with the crack pattern already existing in the palace (e.g. the crack vertically oriented along the north wall) indicating that some of the damaging mechanisms may be already activated. Finally, the lower value of k_8 (vertical walls along the x direction) with respect to k_9 (R9 the vertical walls along the y direction) is probably due to the marked torsional effects suffered by the complex architectural composition of the Consoli Palace.

The results in terms of MAC, Δf and global mode shapes between the FE model and the reference values extracted from the AVT are illustrated in Fig. 7. From the figure it can be noted that MAC values are higher than 0.7 for the first 5 modes and Δf are smaller than 4 %. In order to make the procedure

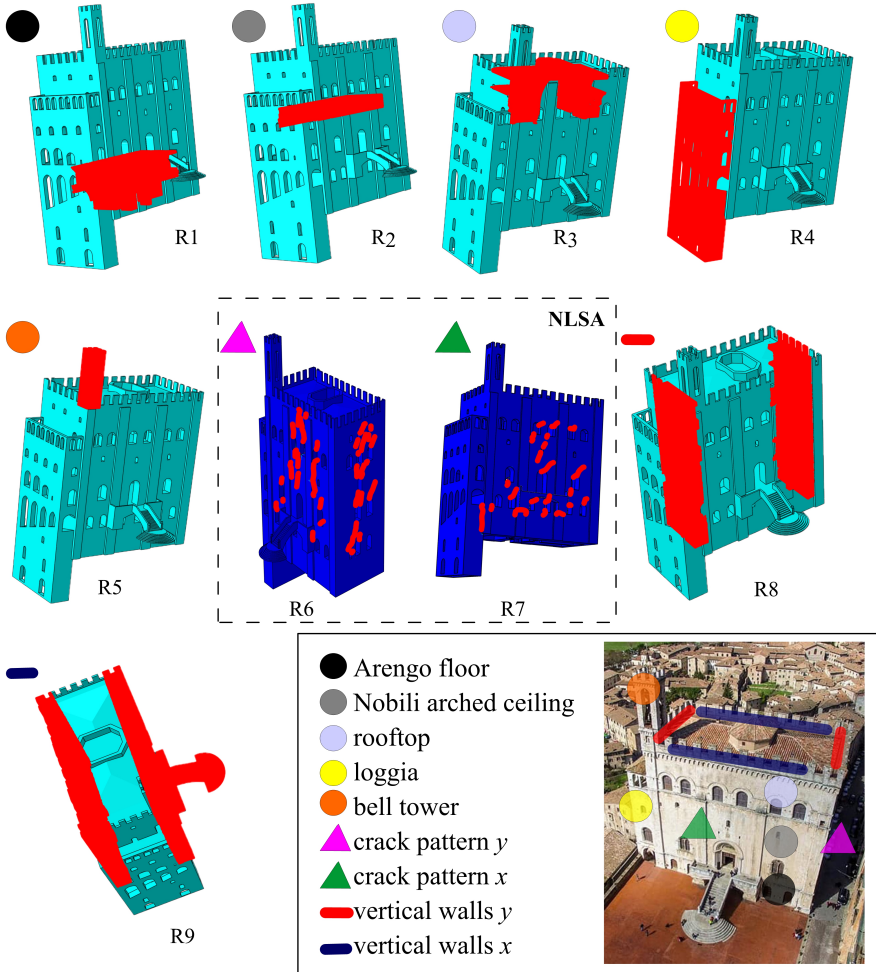


Fig. 6 Selected regions with reference to both FE model and real structure (in red): R1, R2, R3, R4, R5, R6, R7, R8, R9.

computational-effective, a surrogate model is calibrated with a total number of 1000 samples (N_s) randomly simulated for the uncertain parameters collected in vector \mathbf{X} . The surrogate is proposed to reproduce the numerical relationship between FE-based frequencies and mode shapes and uncertain parameters \mathbf{X} . The correspondence of the models is confirmed by the values of R^2 and J_{MAC} evaluated from the FE model and the Kriging model and reported in Table 7. Hence, the surrogate model is assumed as the reference model for the numerical analyses.

The AVTs allow to well characterize the dynamic behavior of the building, given the relatively large number of adopted sensors (19 channels). Fig. 8a)

Region	E [MPa]	k_j	ν	ρ [t/m ³]
1	3510	1	0.34	1.9
2	3327	1	0.34	1.9
3	3327	1	0.34	1.9
4	3327	0.8	0.34	1.9
5	3450	1.4	0.34	1.9
6	3327	0.6	0.34	1.9
7	3327	0.6	0.34	1.9
8	3327	0.65	0.34	1.9
9	3327	1.22	0.34	1.9

Table 6 Nominal values of parameters associated to the FE model-based macro-elements and k_j values after calibration.

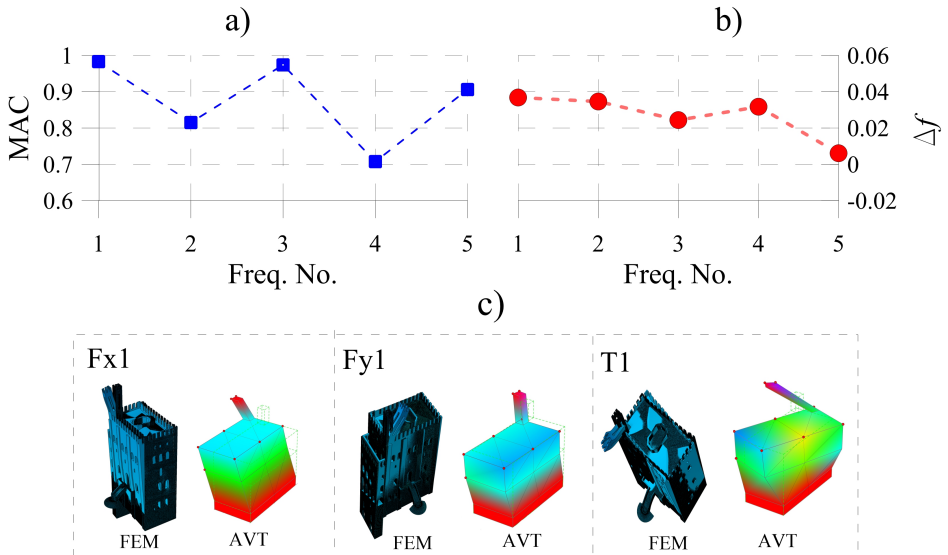


Fig. 7 Results of FE model calibration with respect to AVT: a) MAC; b) Δf ; c) global mode shapes: Fx1, Fy1 and T1.

Parameter	f_1	f_2	f_3	f_4	f_5
R^2	0.999	0.989	0.989	0.995	0.994
J_{MAC}	0.997	0.984	0.995	0.997	0.996

Table 7 Calibration of surrogate model: values of R^2 and J_{MAC} for frequencies f_1 , f_2 , f_3 , f_4 , f_5 .

represents the relative difference Δf between the surrogate nominal frequencies and those evaluated by simulating a possible damage, i.e. considering a reduction of the Young's Modulus of each region of 20%, separately. For instance, the Δf values of region no. 1 are evaluated by considering $k_1 = 0.8$

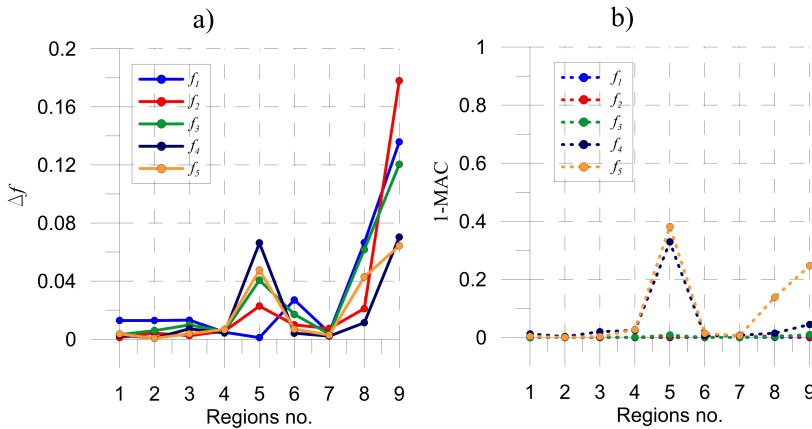


Fig. 8 Frequencies's percentage difference and MAC modification as a function of regions R1-R9 corresponding to $k = 0.8$ (stiffness reduction of 20 %): a) Δf ; b) MAC.

and $k_2, \dots, k_9 = 1$. The term Δf is evaluated as follows:

$$\Delta f = -\frac{f_{\text{sur}} - f_{\text{nom}}}{f_{\text{sur}}} \quad (11)$$

where the negative sign means that a positive value of Δf entails a frequency decay. As expected, the simulation of a damage occurrence induces a certain value of frequency decay (positive Δf) for each region. Fig. 8b) shows the 1-MAC values evaluated between the nominal mode shapes and those corresponding to the simulated damage. More in depth, a graphical representation of the frequencies and MAC which are mostly affected by the damage occurrence within the j th region is illustrated in Table 8, where the color black stands for strongly dependent (Δf higher than 4% and 1-MAC higher than 0.2) and the color light gray for slightly dependent (Δf less than 1% and 1-MAC approximately 0). From the figure it can be depicted that a reduction of k_5 (bell tower) strong influences the dynamic behavior of the building, confirming that global modes has a local component.

Region	Fx1		Ly1		Lx1		Fy1		T1	
	f_1	MAC	f_2	MAC	f_3	MAC	f_4	MAC	f_5	MAC
1	■									
2	■				■					
3	■				■					
4										■
5			■	■	■	■	■	■	■	■
6	■				■					
7			■							
8	■		■		■		■		■	■
9	■		■		■		■	■	■	■

Table 8 Qualitative representation of frequency decay and MAC modification for each region in the case of $k_j = 0.6$.

4 Results and discussion

For the validation of the proposed methodology, monitored data recorded between April 22nd and May 29th of 2021 are analyzed (40 days). The damage detection focuses on the possible consequences related to the seismic sequence occurred on May 15th 2021, with epicenter in Gubbio and a strongest shock of magnitude Mw 4.0 at 07:56 UTC. The other 5 slight shocks occurred between May 15th and May 23rd registered a maximum value of Mw equal to 3.1. Fig. 9a) illustrates the ground acceleration a_g over time of the principal ground motion components recorded by the station "Gubbio Parcheggio Santa Lucia" (GBSL) and available online on the Italian Strong Motion Network (RAN) of the Department of Civil Protection, which provides the data of a dense stations network distributed over the Italian territory (the Italian Seismic Network - RSN of the National Institute of Geophysics and Vulcanology - INGV). Fig. 9b) highlights the geographical location of the epicenter with respect to the Consoli Palace and the station GBSL.

The Δf evaluated comparing the surrogate model's frequencies and those

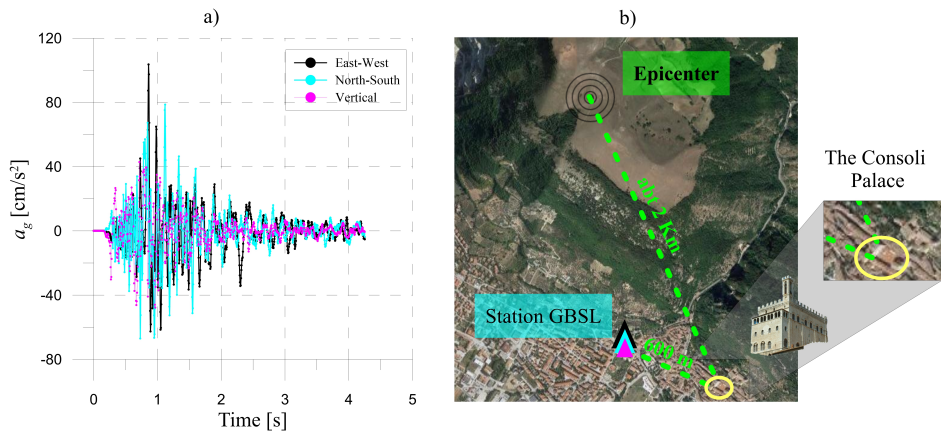


Fig. 9 May 15th earthquake at 7:56 AM: a) a_g over time of the principal ground motion components; b) geographical location of the epicenter with respect to the Consoli Palace and the station GBSL.

identified during the continuous monitoring are depicted in Figs. 10 a)-e) and the corresponding MAC values are reported in Figs. 10 f)-l). From the figure it can be noted that the earthquake occurrence barely affected MAC values, while a positive increase of Δf can be observed, meaning that a frequency decay has occurred to varying degrees for the first five modes. More in detail, the observed frequency decays (FD) are summarized in Table 9.

In order to facilitate the Bayesian-based updating, excluding from the analysis the daily fluctuations, the first five natural frequencies during the investigated 40 days (April 22nd - May 29th) are used and illustrated in Fig. 11. Static measurements recorded by sensors D1 and D2 are here used as a support to visual

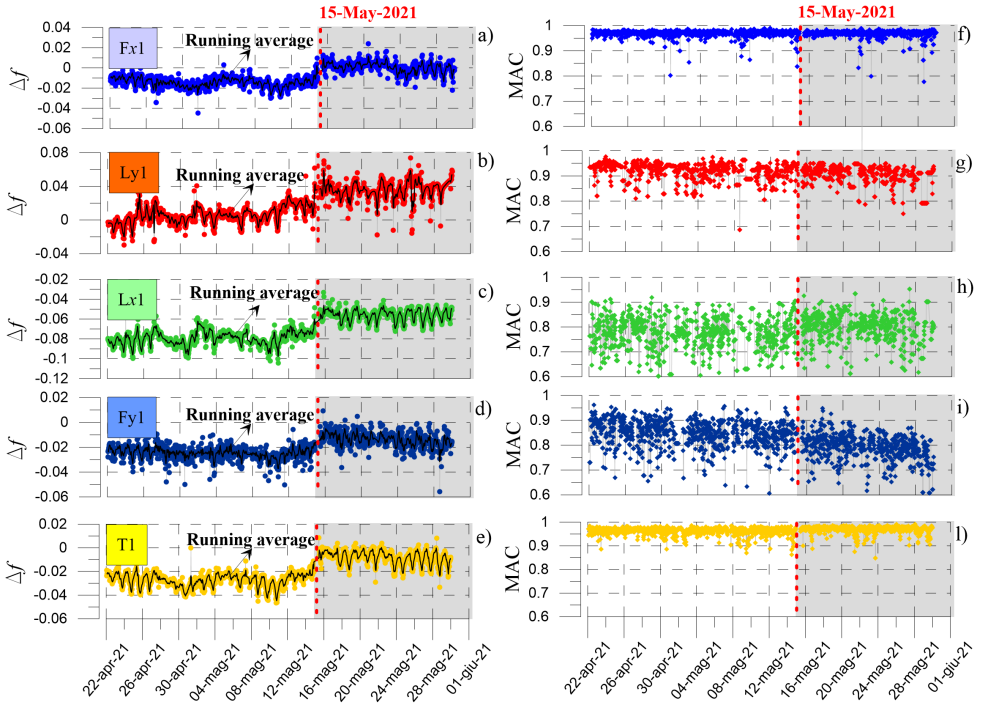


Fig. 10 Continuous monitoring vs surrogate model: a)-e) Δf_j ; f)-l) MAC.

Parameter	f_1	f_2	f_3	f_4	f_5
FD [%]	1.3	2.7	2.3	1.1	1.4

Table 9 Values of frequency decays FD observed after the May seismic sequence.

inspections for data fusion and the residuals of crack amplitudes, evaluated using MLR, can be depicted in Fig. 12. From the figure it can be noted that the mean value of D1 (located within the loggia, i.e., south façade) does not experience significant variations while the trend of D2 (installed in the north façade in correspondence with the major existing crack) exhibits a more evident shift with a closure of about 0.09 mm with no sign of recovering over time, highlighting the appearance of a possible persistent damage in the palace. This result confirms that the main incidence direction of the seismic sequence, i.e., East-West (Fig. 9a), is compatible with an incipient overturning failure mechanism of the western façade, already observed from the existing crack pattern. In this context, a value of $CI=0$ is assigned to R4 (Loggia), and a value of $CI=1$ is assigned to R6 and R8, compatible with possible movement in correspondence of the crack pattern observed along the North façade (R6) and with the incipient mechanism which affects this side of the palace with visible detachment zones between the two orthogonal façades (North-West). It is worth underlying that, in absolute terms, the possible permanent damage experienced by the

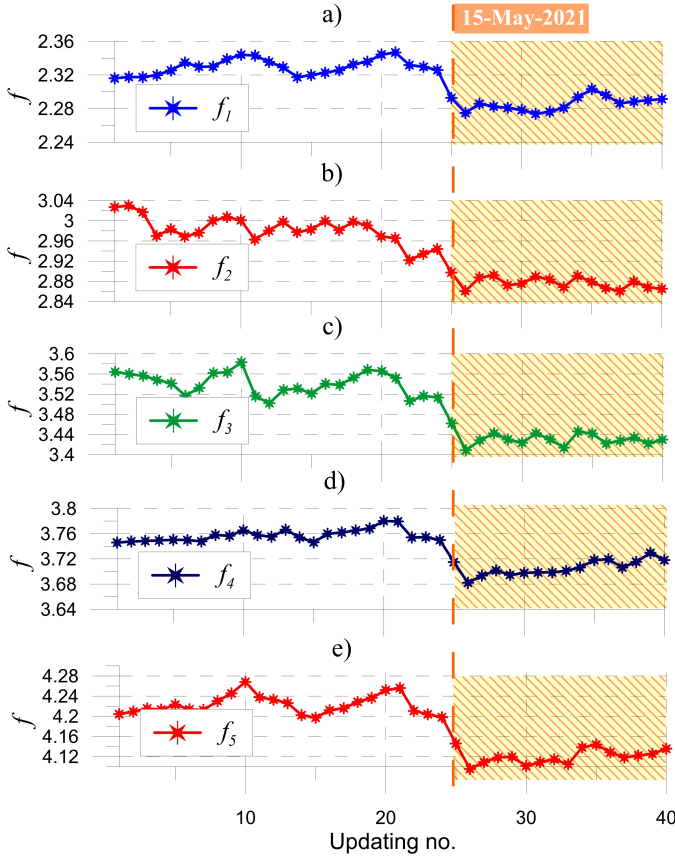


Fig. 11 Daily track of natural frequencies.

structure is not relevant in terms of structural integrity, due to the mild severity of the shock. Fig. 13 illustrates the posterior distributions associated to the uncertain parameters k_1, \dots, k_9 in the undamaged time period (blue lines) and after the May seismic sequence (red lines). With reference to the figure, the mean value of undamaged k_j fluctuates around 1, which indicates that slight variations can daily occur in the frequency and MAC tracking and to the initial FE modeling errors. Then, after the occurrence of the main shock in May 2021, it can be noted that all the uncertain parameters k_j experience a shift of the mean value towards lower values with different severity. This result, consistently with Table 8, highlights that a possible damage is frequency-related. In particular, the results show a significant influence on Regions 3, 6, 7, 8 with a bigger reduction k_j^{up} , i.e., about 30% for R6 and about 20% for R3, R7 and R8. The remaining regions exhibit smaller reductions, less than 10%. Hence a value of BI=1 is assigned to R1,R2,R3,R4,R6,R7 and R8, while the remaining regions (R5 and R9) are scored with BI=0. The Bayesian-based results confirm

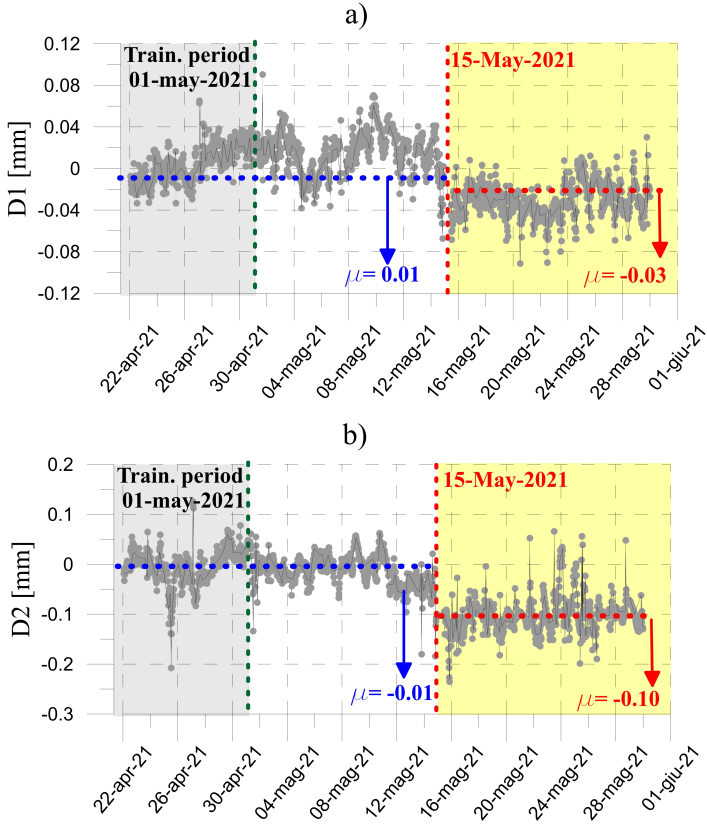


Fig. 12 Residuals of crack amplitudes evaluated using MLR: a) D1; b) D2.

that the possible permanent mild damage, might be related to existing mechanisms already activated within the palace and related to the observed crack pattern. Figs. 14 a)-b) illustrate the values of k_j^{up} and P_j^{dam} over the number of updates. According to Eq. (7), the evaluation of P_j^{dam} depends on the value of the selected damage threshold \bar{k}_j associated with each region, whose values are assumed as follows:

- $\bar{k}_j = 0.4$, $j = 1, 2, 3, 4, 5, 8, 9$, corresponding to a reduction of 40%,
- $\bar{k}_j = 0.7$, $j = 6, 7$ corresponding to a reduction of 70%, since regions R6 and R7 simulate a possible open stage of the local cracks and, consequently, the fully open stage could happen and would correspond to a 100% reduction in Young's modulus.

Hence, on the basis of the selected thresholds \bar{k}_j , the small value of the damage probability associated with R6 and R7 confirms the occurrence of a mild severity damage.

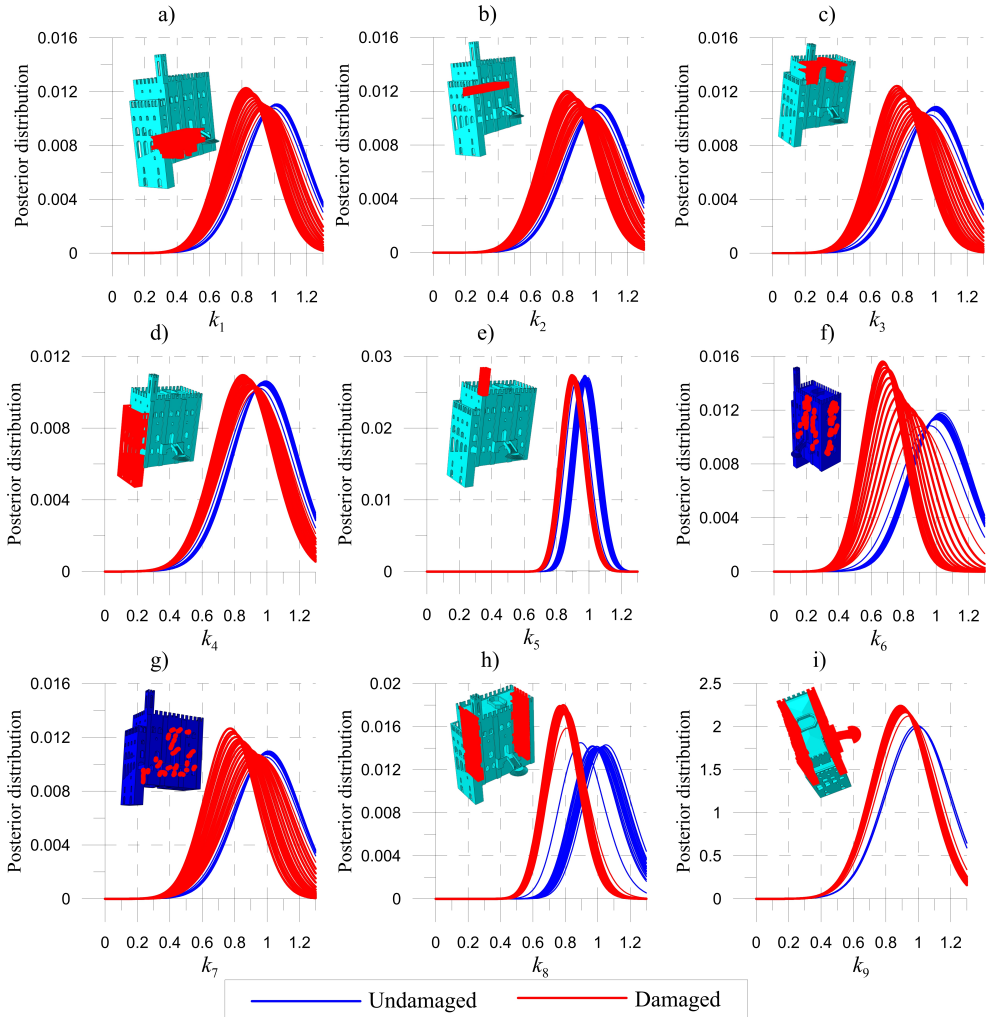


Fig. 13 Bayesian-based posterior distributions: a) k_1 ; b) k_2 ; c) k_3 ; d) k_4 ; e) k_5 ; f) k_6 ; g) k_7 ; h) k_8 ; i) k_1 .

In order to give a correct interpretation to the simulated results, which can be affected by uncertainties because of ill-conditioning issues, measurement noise, sampling process, sensors offset or miscalibration, an in-situ visual inspection has been performed after the main shock. The results of the inspection survey are depicted in Fig. 15. More in detail, Fig. 15a) illustrates the crack visible from the Arengo floor in correspondence of the North wall openings. This damage pattern can be associated with the existing continuous vertical crack that raises from the ground up to the roof on the North façade, as well as several detachment zones between the West façade and internal walls and vaults at the Campanari floor and rooftop. The following scores are assigned to this damage: $G=1$ $K1=0.2$ and $K2=0.2$ and associated with R6 and R7.

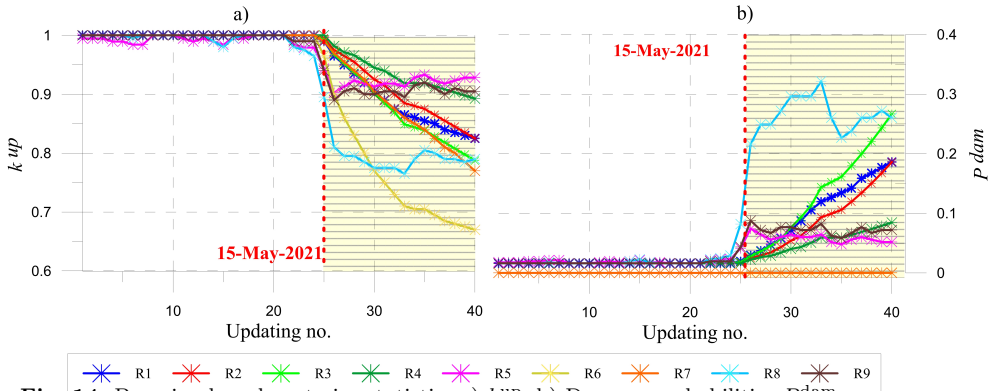


Fig. 14 Bayesian-based posterior statistics: a) k^{up} ; b) Damage probabilities P^{dam} .

Fig. 15b) illustrates some visible cracks originated above and under the opening located within the Loggia's south wall in correspondence of the Arengo floor. The observed cracks are scored with $G=1$ $K1=0.2$ and $K2=0.2$ and are associated with R4. Figs. 15c)-d) show the trend of a continuous crack which propagates from Arengo floor (Fig. 15c) up to the Nobili floor (Fig. 15d) in correspondence of the South façade, accessible from the Loggia. The two portions of the South façade are both scored with $G=1$ $K1=0.2$ and $K2=0.2$ and are associated with R8. The corresponding DI values, calculated according to Eq. (9), are summarized in Table 10.

The results of the data fusion in terms of DI, CI, BI and 2oo3 voter are summarized in Table 10, which confirms that a possible permanent mild severity damage concerns regions R4, R6, R7, R8 (2oo3 voter equal to 1), with a consequent slight modification of the dynamic properties of the palace.

Parameter	R1	R2	R3	R4	R5	R6	R7	R8	R9
DI	0	0	0	0.04	0	0.04	0.04	0.08	0
CI	-	-	-	0	-	1	-	1	-
BI	1	1	1	1	0	1	1	1	0
2oo3 voter	0	0	0	1	0	1	1	1	0

Table 10 Data fusion: DI, CI, BI and 2oo3 voter.

Then, Figs. 16 a)-e) illustrate the updated values of the uncertain parameters k_j^{up} after data fusion over the number of updates, while Figs. 16 f)-l) show the trend of DF vs P^{dam} for the regions characterized by 2oo3 voter = 0. The results of the sole Bayesian model updating are designated as w/o VI and those referring to the data fusion are designated as VI. On the one hand, from the w/o VI cases it can be confirmed that the May seismic sequence induces ambiguous results (possible false alarms) in the structure with an increased value of P^{dam} and/or DF for all the selected regions. Then, the data fusion allows to adjust the Bayesian model updating with a reduction of

P^{dam} and DF, as reported in Figs. 16 f)-l).

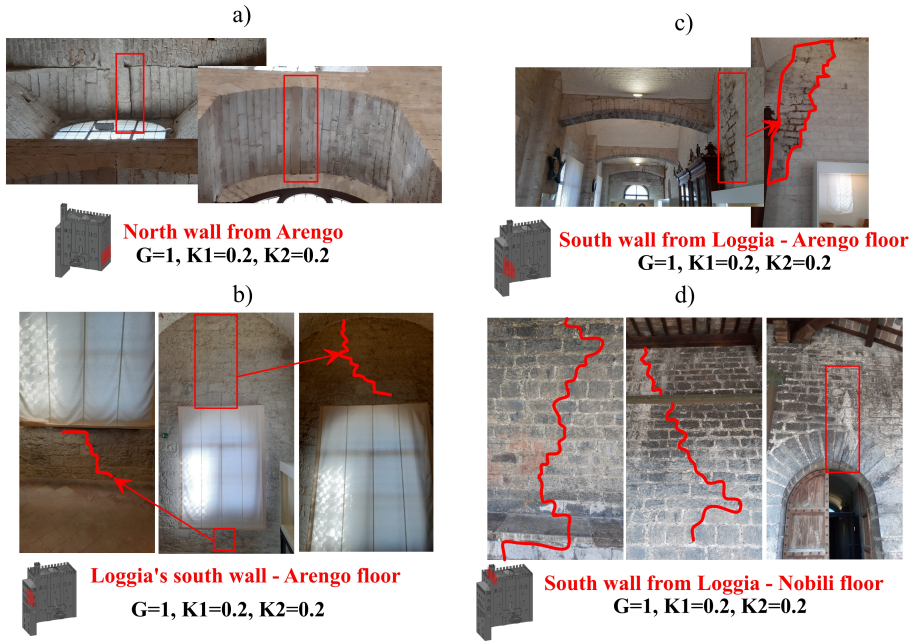


Fig. 15 Post-earthquake results of visual inspections: a) North wall from Arengo; b) Loggia's south wall (Arengo floor); c) South wall of the palace from Loggia (Arengo floor); c) South wall of the palace from Loggia (Nobili floor);.

Furthermore, Figs. 17 a)-d) illustrate the time series of k^{up} and P^{dam} over the number of updates for the regions characterized by $2003 \text{ voter} = 1$, i.e., whose updated results are confirmed by visual inspections and static measurements (if informative). Hence, the results confirm a possible permanent, but very limited, damage in regions R4, R6, R7, R8, with values of P^{dam} far from the alarm state (red dot lines).

Finally, in Fig. 18 is depicted the damage map in the case of the sole Bayesian model updating vs data fusion with the indication of the color's map on the basis of k_j^{up} . The damage map confirms that a data fusion approach allows to mitigate uncertainties and to overcome the ill-conditioned Bayesian model updating in the damage assessment process, excluding those areas which have no evidence of damage.

5 Conclusions

A Bayesian-based data fusion methodology has been presented with the aim of detecting and locating post-earthquake structural damages in monumental structures by making use of both monitoring data and visual inspections, also including FE and surrogate modeling. The main advantages and innovations of the proposed methodology concern: (i) the combination of different

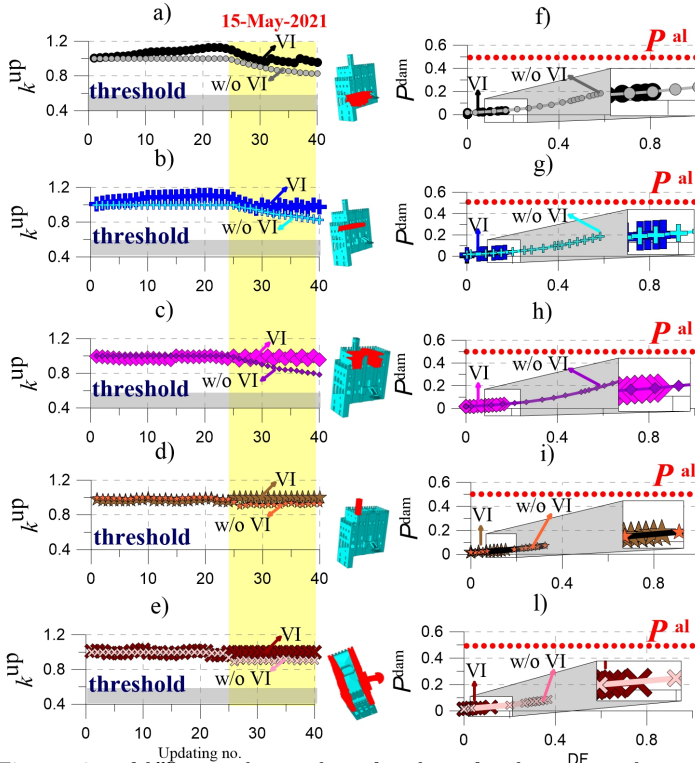


Fig. 16 Time series of k^{up} over the number of updates for the regions characterized by 2003 voter = 0, with the indication of the k threshold and trend of DF vs P^{dam} with the indication of P^{al} : a)-f) R1; b)-g) R2; c)-h) R3; d)-i) R5; e)-l) R9.

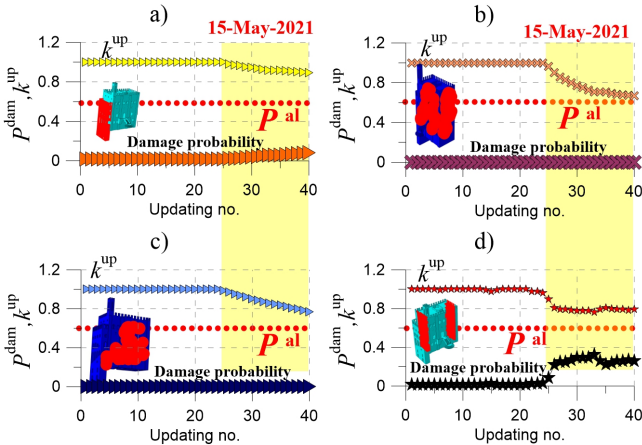


Fig. 17 Time series of k^{up} and P^{dam} over the number of updates for the regions characterized by 2003 voter = 1: a) R4; b) R6; c) R7; d) R8.

sources of information using Bayesian inference; (ii) the probability-based

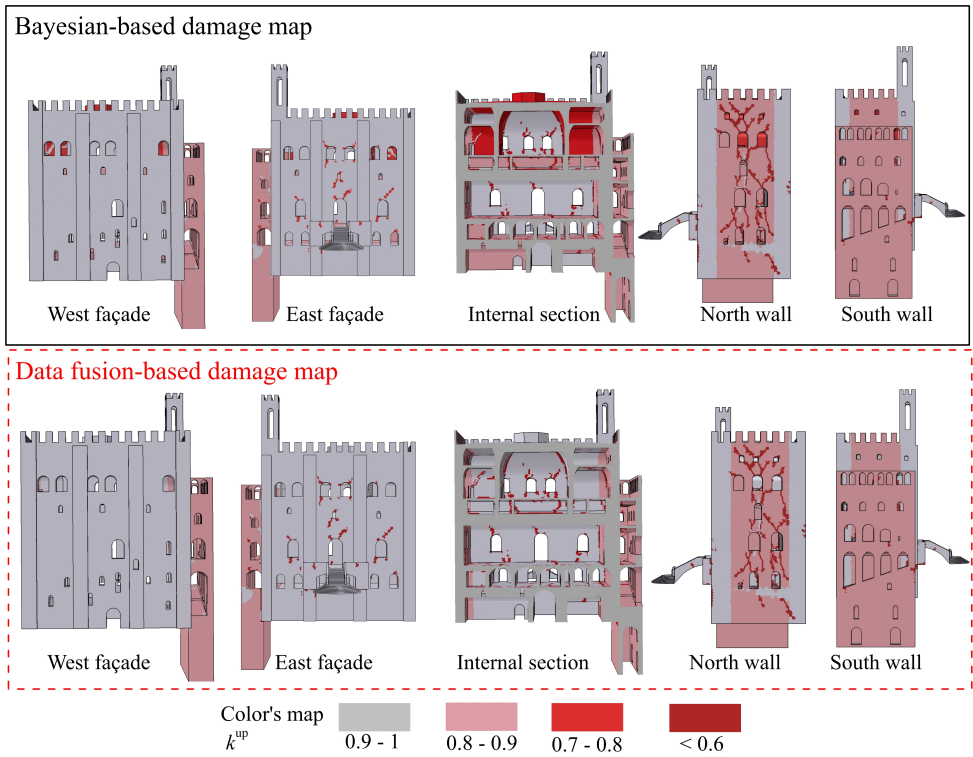


Fig. 18 Bayesia-based vs Data fusion-based damage map.

simulation to handle uncertainties; (iii) the use of simplified and computationally effective numerical models. The case study building is the Consoli Palace (Umbria, Italy), an historical masterpiece equipped with a permanent monitoring system since 2017, which was hit by low-intensity earthquakes in 2021. In order to demonstrate the efficacy of the proposed procedure, a computationally-effective FE model and a reduced-dimensional surrogate model able to reproduce the dynamic behavior of the palace are built. Damage-sensitive regions within the structure are identified by means of non-linear static analyses and engineering judgment. Each region is defined as a one-parameter dependent, the parameter being the multiplier k_j of all elastic constants assigned to the isotropic materials associated with the j th region. Then, an on-line data fusion approach is proposed by linking the Bayesian model updating, the static measurements and the results of visual inspections enabling to continuously identify a possible damage over the selected regions. The data fusion results allow to explore the implications of all factors that shape and constrain decision making, to highlight the importance of plan inspection surveys in monumental structures and to accurately evaluate intervention options and establish priorities in a structured context (selected damaged-prone regions), avoiding the possible detection of false alarms.

Acknowledgments. The Authors would like to acknowledge the support of the PRIN 2017 project, "DETECT-AGING" (Prot. 201747y73L), funded by the Italian Ministry of University and Research.

Declarations

- Funding
- Conflict of interest/Competing interests (check journal-specific guidelines for which heading to use)
- Ethics approval
- Consent to participate
- Consent for publication
- Availability of data and materials
- Code availability
- Authors' contributions

References

- [1] Farrar, C.R., Worden, K.: An introduction to structural health monitoring. *Philosophical Transactions of the Royal Society A* **365**(1851), 303–315 (2007). <https://doi.org/10.1098/rsta.2006.1928>
- [2] Farrar, C.R., Worden, K.: Structural health monitoring: A machine learning perspective. John Wiley & Sons, Ltd. (2012). <https://doi.org/10.1002/9781118443118>
- [3] Kaya, Y., Safak, E.: Real-time analysis and interpretation of continuous data from structural health monitoring (SHM) systems. *Bulletin of Earthquake Engineering* **13**(3), 917–934 (2015)
- [4] Cavalagli, N., Comanducci, G., Ubertini, F.: Earthquake-induced damage detection in a monumental masonry bell-tower using long-term dynamic monitoring data. *Journal of Earthquake Engineering* **22**, 96–119 (2018)
- [5] Downey, A., D'Alessandro, A., Laffamme, S., Ubertini, F.: Smart bricks for strain sensing and crack detection in masonry structures. *Smart Materials and Structures* **27**(1), 015009 (2018)
- [6] Venanzi, I., Kita, A., Cavalagli, N., Ierimonti, L., Ubertini, F.: Earthquake-induced damage localization in an historic masonry tower through long-term dynamic monitoring and fe model calibration. *Bulletin of Earthquake Engineering* **18**(5), 2247–2274 (2020)
- [7] Sivori, D., Cattari, S., Lepidi, M.: A methodological framework to relate the earthquake-induced frequency reduction to structural damage in masonry buildings. *Bulletin of Earthquake Engineering* (2022). in Press

- [8] Kita, A., Cavalagli, N., Ubertini, F.: Temperature effects on static and dynamic behavior of consoli palace in gubbio, italy. *Mechanical Systems and Signal Processing* **120**, 180–202 (2019)
- [9] Behmanesh, I., Moaveni, B., Lombaert, G., Papadimitriou, C.: Hierarchical bayesian model updating for structural identification. *Mechanical Systems and Signal Processing* **64–65**, 360–376 (2015)
- [10] Behmanesh, I., Moaveni, B.: Accounting for environmental variability, modeling errors, and parameter estimation uncertainties in structural identification. *Journal of Sound and Vibration* **374**, 92–110 (2016)
- [11] Sun, H., Mordret, A., Prieto, G.A., Toksz, M.N., Bykztrk, O.: Bayesian characterization of buildings using seismic interferometry on ambient vibrations. *Mechanical Systems and Signal Processing* **85**, 468–486 (2017)
- [12] Rocchetta, R., Broggi, M., Huchet, Q., Patelli, E.: On-line bayesian model updating for structural health monitoring. *Mechanical Systems and Signal Processing* **103**, 174–195 (2018). <https://doi.org/10.1016/j.ymsp.2017.10.015>
- [13] Bartoli, G., Betti, M., Marra, A.M., Monchetti, S.: A bayesian model updating framework for robust seismic fragility analysis of non-isolated historic masonry towers. *Philosophical Transactions of the Royal Society A: Mathematical, Physical and Engineering Sciences* **377**(2155), 20190024 (2019)
- [14] Ierimonti, L., Venanzi, I., Cavalagli, N., Comodini, F., Ubertini, F.: An innovative continuous bayesian model updating method for base-isolated RC buildings using vibration monitoring data. *Mechanical Systems and Signal Processing* **139**, 106600 (2020)
- [15] Tibaduiza Burgos, D.A., Gomez Vargas, R.C., Pedraza, C., Agis, D., Pozo, F.: Damage identification in structural health monitoring: A brief review from its implementation to the use of data-driven applications. *Sensors (Switzerland)* **20**(3), 733 (2020)
- [16] Ierimonti, L., Venanzi, I., García-Macías, E., Ubertini, F.: A transfer bayesian learning methodology for structural health monitoring of monumental structures. *Engineering Structures* **247**(113089) (2021). <https://doi.org/10.1016/j.engstruct.2021.113089>
- [17] Simoen, E., De Roeck, G., Lombaert, G.: Dealing with uncertainty in model updating for damage assessment: A review. *Mechanical Systems and Signal Processing* **56–57**, 123–149 (2015)
- [18] Yuen, K.-V., Katafygiotis, L.S.: Bayesian time-domain approach for

- modal updating using ambient data. *Probabilistic Engineering Mechanics* **16**(3), 219–231 (2001)
- [19] Au, S.-K.: Uncertainty law in ambient modal identification-part ii: Implication and field verification. *Mechanical Systems and Signal Processing* **48**(1-2), 34–48 (2014)
- [20] Yan, W.-J., Katafygiotis, L.S.: An analytical investigation into the propagation properties of uncertainty in a two-stage fast bayesian spectral density approach for ambient modal analysis. *Mechanical Systems and Signal Processing* **118**, 503–533 (2019)
- [21] Beck, J.L., Katafygiotis, L.S.: Updating models and their uncertainties. i: Bayesian statistical framework. *Journal of Engineering Mechanics* **124**(4), 455–461 (1998). [https://doi.org/10.1061/\(ASCE\)0733-9399\(1998\)124:4\(455\)](https://doi.org/10.1061/(ASCE)0733-9399(1998)124:4(455))
- [22] Yuen, K.V.: *Bayesian methods for structural dynamics and civil engineering*. John Wiley & Sons (Asia), Singapore (2010)
- [23] García-Macías, E., Ierimonti, L., Venanzi, I., Ubertini, F.: An innovative methodology for online surrogate-based model updating of historic buildings using monitoring data. *International Journal of Architectural Heritage* **15**(1), 92–112 (2019)
- [24] García-Macías, E., Ierimonti, L., Venanzi, I., Ubertini, F.: Comparison of surrogate models for handling uncertainties in SHM of historic buildings. *Proceeding of XXIV Aimeta Conference*, 1645–1657 (2020)
- [25] Neves, A.C., Gonzalez, I., Leander, J., Karoumi, R.: Structural health monitoring of bridges: a model-free ann-based approach to damage detection. *Journal of Civil Structural Health Monitoring* **7**(5), 689–702 (2017)
- [26] Neves, A.C., González, I., Leander, J., Karoumi, R.: A new approach to damage detection in bridges using machine learning. *Lecture Notes in Civil Engineering* **5**, 73–84 (2018)
- [27] Sun, L., Shang, Z., Xia, Y., Bhowmick, S., Nagarajaiah, S.: Review of bridge structural health monitoring aided by big data and artificial intelligence: From condition assessment to damage detection. *Journal of Structural Engineering (United States)* **146**(5) (2020)
- [28] Bull, L.A., Rogers, T.J., Wickramarachchi, C., Cross, E.J., Worden, K., Dervilis, N.: Probabilistic active learning: An online framework for structural health monitoring. *Mechanical Systems and Signal Processing* **134**, 106294 (2019)

- [29] Bull, L.A., Worden, K., Dervilis, N.: Towards semi-supervised and probabilistic classification in structural health monitoring. *Mechanical Systems and Signal Processing* **140**, 106653 (2020)
- [30] Khaleghi, B., Khamis, A., Karray, F.O., Razavi, S.N.: Multisensor data fusion: A review of the state-of-the-art. *Information Fusion* **14**(1), 28–44 (2013). <https://doi.org/10.1016/j.inffus.2011.08.001>
- [31] Wu, R.-T., Jahanshahi, M.R.: Data fusion approaches for structural health monitoring and system identification: Past, present, and future. *Structural Health Monitoring* **19**(2), 552–586 (2020). <https://doi.org/10.1177/1475921718798769>
- [32] Kralovec, C., Schagerl, M.: Review of structural health monitoring methods regarding a multi-sensor approach for damage assessment of metal and composite structures. *Sensors (Switzerland)* **20**(3), 826 (2020)
- [33] Hall, D.L., Llinas, J.: An introduction to multi-sensor data fusion. *Proceedings of the IEEE* **85**(1) (1997). <https://doi.org/10.1109/5.554205>
- [34] Chatzis, M.N., Chatzi, E.N., Smyth, A.W.: An experimental validation of time domain system identification methods with fusion of heterogeneous data. *Earthquake Engineering and Structural Dynamics* **44**(4), 523–547 (2015). <https://doi.org/10.1002/eqe.2528>
- [35] Downey, A., Ubertini, F., Laflamme, S.: Algorithm for damage detection in wind turbine blades using a hybrid dense sensor network with feature level data fusion. *Journal of Wind Engineering and Industrial Aerodynamics* **168**, 288–296 (2017). <https://doi.org/10.1016/j.jweia.2017.06.016>
- [36] Jiang, S.-F., Zhang, C.-M., Zhang, S.: Two-stage structural damage detection using fuzzy neural networks and data fusion techniques. *Expert Systems with Applications* **38**(1), 511–519 (2011). <https://doi.org/10.1016/j.eswa.2010.06.093>
- [37] Lenjani, A., Dyke, S.J., Bilonis, I., Yeum, C.M., Kamiya, K., Choi, J., Liu, X., Chowdhury, A.G.: Towards fully automated post-event data collection and analysis: Pre-event and post-event information fusion. *Engineering Structures* **208**, 109884 (2020)
- [38] Li, X.Y., Lin, S.J., Law, S.S., Lin, Y.Z., Lin, J.F.: Fusion of structural damage identification results from different test scenarios and evaluation indices in structural health monitoring. *Structural Health Monitoring* (2020). –in Press
- [39] Mohamadi, S., Lattanzi, D., Azari, H.: Fusion and visualization of bridge

- deck nondestructive evaluation data via machine learning. *Frontiers in Materials* **7**, 576918 (2020)
- [40] Rabiei, M., Modarres, M.: A recursive bayesian framework for structural health management using online monitoring and periodic inspections. *Reliability Engineering and System Safety* **112**, 154–164 (2013). <https://doi.org/10.1016/j.res.2012.11.020>
- [41] Ramos, L.F., Miranda, T., Mishra, M., Fernandes, F.M., Manning, E.: A bayesian approach for NDT data fusion: The Saint Torcato church case study. *Engineering Structures* **84**, 120–129 (2015)
- [42] Sun, X.D., Sun, X.Y., He, J., Hou, G.L.: Bayesian-based structural damage detection on the integration of global and local information. *Advances in Structural Engineering* **18**(4), 543–553 (2015). <https://doi.org/10.1260/1369-4332.18.4.543>
- [43] Zhao, X., Wang, R., Gu, H., Song, G., Mo, Y.L.: Innovative data fusion enabled structural health monitoring approach. *Mathematical Problems in Engineering* **2014** (2014). <https://doi.org/10.1155/2014/369540>
- [44] Lophaven, S.N., Nielsen, H.B., Søndergaard, J.: A matlab kriging toolbox, version 2.0. Technical Report IMM-TR-2002-12, Kongens Lyngby, Copenhagen, Denmark: Informatics and Mathematical Modelling, Technical University of Denmark, DTU. (2002)
- [45] Steel, R.-G.-D., Torrie, J.-H.: Principles and procedures of statistics with special reference to the biological sciences. McGraw Hill (1960)
- [46] García-Macías, E., Ubertini, F.: MOVA/MOSS: Two integrated software solutions for comprehensive structural health monitoring of structures. *Mechanical Systems and Signal Processing* **143**, 106830 (2020)
- [47] Ubertini, F., Carmelo, G., Materazzi, A.L.: Automated modal identification in operational conditions and its application to bridges. *Engineering Structures* **46**, 264–278 (2013)
- [48] Efron, B., Hastie, T., Johnstone, I., Tibshirani, R.: Least angle regression. *Annals of statistics* **32**(2), 407–499 (2004)
- [49] Hotteling, H.: Multivariate quality control, illustrated by the air testing of sample bombsights. *Techniques of statistical analysis*, 111–184 (1947)
- [50] Jang, J., Smyth, A.: Bayesian model updating of a full-scale finite element model with sensitivity-based clustering. *Structural Control and Health Monitoring* **24**(11) (2017)

- [51] Vanik, M.W., Beck, L.J., Au, S.K.: Bayesian Probabilistic Approach to Structural Health Monitoring. *Journal of Engineering Mechanics* **126**(7) (2000)
- [52] Sezen, H., Dogangun, A.: Earthquake engineering: Seismic performance of historical and monumental structures. IntechOpen (2012). <https://doi.org/10.5772/51338>
- [53] Indirli, M., Kouris, L.A.S., Formisano, A., Borg, R.P., Mazzolani, F.M.: Seismic damage assessment of unreinforced masonry structures after the Abruzzo 2009 earthquake: The case study of the historical centers of l'Aquila and Castelvechio subequo. *International Journal of Architectural Heritage* **7**(5), 536–578 (2013)
- [54] Zuccaro, G., Cacace, F., Rauci, M.: Medea: A multimedia and didactic handbook for structural damage and vulnerability assessment - l'Aquila case study. COST ACTION C26: Urban Habitat Constructions under Catastrophic Events - Proceedings of the Final Conference, 747–754 (2010)
- [55] Akgl, F., Frangopol, D.M.: Bridge rating and reliability correlation: Comprehensive study for different bridge types. *Journal of Structural Engineering* **130**(7), 1063–1074 (2004)
- [56] Medina, P., Gonzalez, J.L.: Reinforced concrete long-term deterioration prediction for the implementation of a bridge management system. *Materials Today: Proceedings* **58**(4), 1265–1271 (2022)
- [57] Applied Technology Council (ATC): Atc-20, procedures for post-earthquake safety evaluation of buildings. Redwood City, California. (1989)
- [58] Applied Technology Council (ATC): Atc 20-2, addendum to the atc-20 post-earthquake building safety evaluation procedures (revised in early 2005). Redwood City, California. (1995)
- [59] Applied Technology Council (ATC): Atc 20-3, case studies in rapid post-earthquake safety evaluation of buildings. Redwood City, California. (1996)
- [60] Flammini, F., Marrone, S., Mazzocca, N., Nardone, R., Vittorini, V.: Using Bayesian Networks to Evaluate the Trustworthiness of '2 Out of 3' Decision Fusion Mechanisms in Multi-sensor Applications, vol. 28, pp. 682–687 (2015). <https://doi.org/10.1016/j.ifacol.2015.09.606>
- [61] Ministero delle infrastrutture e dei trasporti (MIT): Norme Tecniche per Le Costruzioni., (2018)

- [62] Mirabella, F., Ciaccio, M.G., Barchi, M.R., Merlini, S.: The gubbio normal fault (central italy): Geometry, displacement distribution and tectonic evolution. *Journal of Structural Geology* **26**(12), 2233–2249 (2004)
- [63] Chiaraluze, L., Amato, A., Carannante, S., Castelli, V., Cattaneo, M., Cocco, M., Collettini, C., DAlema, E., Di Stefano, R., Latorre, D., Marzorati, S., Mirabella, F., Monachesi, G., Piccinini, D., Nardi, A., Piersanti, A., Stramondo, S., Valoroso, L.: The alto tiberina near fault observatory (northern apennines, italy). *Annals of Geophysics* **57**(3) (2014). <https://doi.org/10.4401/ag-6426>
- [64] Cavalagli, N., Kita, A., Castaldo, V.L., Pisello, A.L., Ubertini, F.: Hierarchical environmental risk mapping of material degradation in historic masonry buildings: An integrated approach considering climate change and structural damage. *Construction and Building Materials* **215**, 998–1014 (2019)
- [65] García-Macías, E., Ubertini, F.: Least angle regression for early-stage identification of earthquake-induced damage in a monumental masonry palace: Palazzo dei consoli. *Engineering Structures* **259**, 114119 (2022). <https://doi.org/10.1016/j.engstruct.2022.114119>
- [66] Lubliner, J., Oliver, J., Oller, S., Oate, E.: A plastic-damage model for concrete. *International Journal of Solids and Structures* **25**(3), 299–326 (1989)